ACSNANO

www.acsnano.org

ARTICLE

Pushing the Limits on the Intestinal Crossing of Metal–Organic Frameworks: An *Ex Vivo* and *In Vivo* Detailed Study

Sara Rojas, Tania Hidalgo, Zhongrui Luo, David Ávila, Anna Laromaine,* and Patricia Horcajada*

Cite This: *ACS Nano* 2022, 16, 5830–5838

Read Online

ACCESS | Metrics & More | Article Recommendations | Supporting Information

ABSTRACT: **Biocompatible nanoscaled metal–organic frameworks (nanoMOFs) have been widely studied as drug delivery systems (DDSs), through different administration routes, with rare examples in the convenient and commonly used oral administration. So far, the main objective of nanoMOFs as oral DDSs was to increase the bioavailability of the cargo, without considering the MOF intestinal crossing with potential advantages (e.g., increasing drug availability, direct transport to systemic circulation). Thus, we propose to address the direct quantification and visualization of MOFs' intestinal bypass. For that purpose, we select the microporous Fe-based nanoMOF, MIL-127, exhibiting interesting properties as a nanocarrier (great biocompatibility, large porosity accessible to different drugs, green and multigram scale synthesis, outstanding stability along the gastrointestinal tract). Additionally, the outer surface of MIL-127 was engineered with the biopolymer chitosan (CS@MIL-127) to improve the nanoMOF intestinal permeation. The biocompatibility and intestinal crossing of nanoMOFs is confirmed using a simple and relevant *in vivo* model, *Caenorhabditis elegans*; these worms are able to ingest enormous amounts of nanoMOFs (up to 35 g per kg of body weight). Finally, an *ex vivo* intestinal model (rat) is used to further support the nanoMOFs' bypass across the intestinal barrier, demonstrating a fast crossing (only 2 h). To the best of our knowledge, this report on the intestinal crossing of intact nanoMOFs sheds light on the safe and efficient application of MOFs as oral DDSs.**

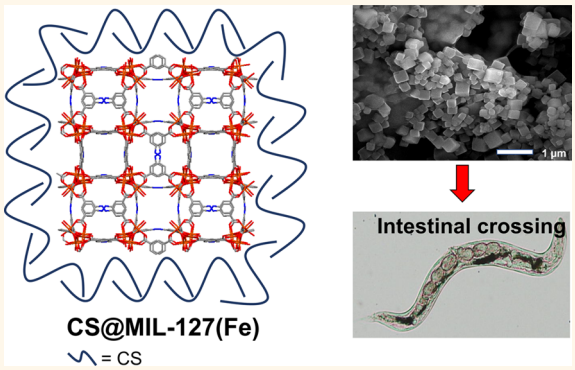

KEYWORDS: *Metal–Organic Frameworks, Chitosan, Intestinal Permeability, Caenorhabditis elegans, Bioavailability*

Drug delivery systems (DDSs) are one of the most promising tools for human healthcare owing to the temporary and local control of drug release. The design of new therapeutic active ingredients (AIs) and intelligent treatments has resulted in the development of a new class of nontoxic carriers, known as metal–organic frameworks (MOFs).[1] MOFs represent an interesting family of hybrid materials, based on metal ions interconnected through organic polydentate linkers,[2] giving rise to an ordered structure of channels and cavities accessible to guest molecules (e.g., AIs). Their outperforming properties (exceptional porosity, versatile structure and composition, selective sorption, tunable particle size and stability, biocompatibility, biodegradation, etc.)[3] made them suitable candidates as DDSs.

In this regard, nanoscaled MOFs (nanoMOFs) have been widely studied as DDSs, addressing in the vast majority of these investigations the intravenous or intraperitoneal routes, with rare examples in oral, pulmonary, cutaneous, or ocular administration.[4−8] Among them, the oral route is one of the most convenient and commonly used routes, since it is simple and noninvasive and avoids patient pain and discomfort, enhancing treatment adherence and, so, efficacy. To the best of our knowledge, no more than nine works have investigated so far the *in vivo* oral administration of MOFs as DDSs, as for instance: a K-cyclodextrin MOF (CD-MOF-1(K)) for the administration of ibuprofen,[9] UiO-66(Zr) in the administration of magnolol,[5] an Al-based MOF in the release of ovalbumin,[10] or, very recently, the use of MIL-100(Fe) in the oral administration of insulin[11] and genistein.[12] Among these studies, the main objective was to increase the bioavailability of

Received: December 9, 2021
Accepted: February 28, 2022
Published: March 17, 2022

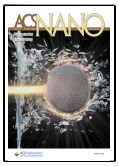

the cargo (using always a rodent model: mouse or rat), without considering the potential intestinal crossing of the intact nanoMOF as a whole carrier, exclusively monitoring the drug or the MOF constituents (cation or ligand). In this regard, it should be noted that there is no report addressing the direct visualization of the nanoMOFs' intestinal bypass.

An efficient carrier intestinal crossing represents important advantages: (*i*) the increasing of the AIs' availability by their protection within the nanocarrier and/or the modification of their physicochemical properties (e.g., solubility), (*ii*) their direct transport to systemic circulation (via hepatic portal or intestinal lymphatic systems), (*iii*) the targeting of macrophages and dendritic cells, being beneficial for oral vaccinations, and/or (*iv*) the passive lymphatic targeting followed by systemic drug delivery.[13] Therefore, this work aims to study the *in vivo* impact of the surface chemistry and particle size/aggregation on the intestinal permeation of MOFs as oral DDSs. We propose here to evaluate the biocompatibility and intestinal bypass of MOFs at the *in vivo* level using a simple and useful animal model, the *Caenorhabditis elegans* (*C.elegans*). The intestine of this nematode possesses some similarities compared to complex organisms, such as humans.[14] In particular, its intestine shares a similar cellular architecture with higher animals with respect to the cell polarity of the intestinal cells (enterocytes), including the presence of apical and basolateral domains, cell junctions, and the presence of microvilli forming the brush border.[15] In this work, we have selected a microporous Fe-nanoMOF denoted as MIL-127,[16] with a cubic structure based on iron(III) octahedra trimers and the 3,3′,5,5′-azobenzenetetracarboxylate anions ($TazBz^{4-}$, noted in the acid form as H_4TazBz), which exhibit interesting properties as a DDS: (*i*) good biocompatibility,[17] (*ii*) porosity accessible to different natural AIs (Brunauer, Emmett, and Teller surface area (S_{BET}) > 1200 $m^2 \cdot g^{-1}$, $V_p \approx 0.7$ $cm^3 \cdot g^{-1}$, with two types of pores, a one-dimensional channel system (~6 Å), and cages of ~10 Å, accessible through narrow apertures of ~3 Å),[18,19] (*iii*) fine control of the particle dimensions from micro to monodispersed nanometric sizes,[20] (*iv*) green and fast multigram scale synthesis,[20] and (*v*) the highest reported chemical stability along the gastrointestinal (GI) track among all the studied MOFs.[21] Additionally, we have evaluated the surface engineering of MIL-127 with the biopolymer chitosan (CS; named CS@MIL-127) as a manner to regulate the potential paracellular transport and/or bioadhesive properties of MIL-127, which could favor its intestinal crossing, as previously shown in other nanomaterials.[22,23] Hence, MIL-127 and CS@MIL-127 nanoparticles (NPs) were first prepared and fully characterized, with particular attention to their structural, chemical, and colloidal stability under simulated physiological oral conditions (Figure 1). Then, the biocompatibility and intestinal crossing of the uncoated and CS-coated nanoMOFs were assessed using the *in vivo* model *C. elegans*. Finally, an *ex vivo* intestinal model (rat) was used to further monitor the MIL-127 and CS@MIL-127 bypass across the intestinal barrier.

RESULTS AND DISCUSSION

Preparation of CS@MIL-127 NPs and Physicochemical Characterization. MIL-127 NPs were synthesized following a previously reported procedure,[25] and the coating of their outer surface was performed using a simple and completely green one-pot impregnation method, adapted from a recent one developed by us and applied to a different

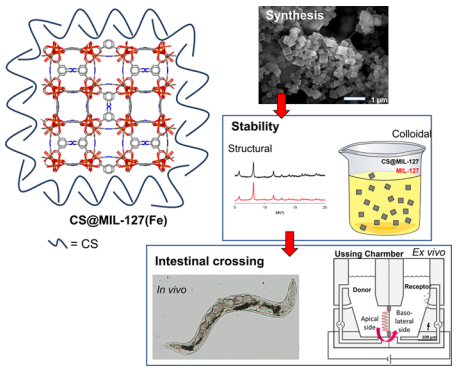

Figure 1. Left: Schematic view of the structure of CS@MIL-127 nanoparticles (NPs) (iron, nitrogen, oxygen, and carbon are represented in orange, blue, red, and gray, respectively; hydrogen atoms are omitted for clarity). Right: Procedure for intestinal crossing evaluation: (top) synthesis of the NPs, showing a scanning electron microscopy (SEM) image (scale bar = 1 μm); (middle) evaluation of the structural, chemical, and colloidal stability under simulated oral conditions, depicting an example of the structural stability in mucin-complemented simulated intestinal fluid (*lis*-SIF-muc); and (bottom) direct observation of the NP bypass in the *C. elegans* model and scheme of a Ussing chamber used in the *ex vivo* experiments with the intestine of rat.[24]

nanoMOF structure (further details of the synthesis in the Experimental Section).[26] The successful grafting and preservation of the MIL-127 NPs' main features were monitored through a set of experimental techniques (see Supporting Information, Sections S1 and S2). The amount of the CS coating was determined by inductively coupled plasma atomic emission spectroscopy (ICP-OES), thermogravimetric analysis (TGA), and elemental analysis (EA), reaching a significant grafting after only 30 min of contact (37.0 wt %, expressed as percentage with respect to the dry NP weight). Further, the X-ray powder diffraction (XRPD) patterns of the obtained polycrystalline powder confirmed that the crystalline structure of MIL-127 NPs was not altered after the surface modification (Figure S2b). To shed light on the nature of the interactions between MIL-127 NPs and the CS moieties, Fourier transform infrared (FTIR) spectroscopy was also performed (Figure S3b,c). Compared with the free CS spectrum as a reference and besides the main bands assigned to MIL-127, the CS@MIL-127 NPs exhibited additional bands at 1145 cm^{-1} corresponding to the N-glycosidic bond, a clear indication of the presence of CS. So far, we have assumed that the polymer lies on the outer surface of the NPs. However, due to the microporous character of MIL-127 NPs, it is plausible that CS due to its size (5.2 × 6.6 × 3.7 $Å^3$) could also be located within the pores of MIL-127. To address this issue, N_2 sorption isotherms were measured at 77 K on coated *vs.* uncoated NPs (Figure S2a). Similar BET surfaces for MIL-127 and CS@MIL-127, after CS weight correction, were obtained (890 *vs.* 876 $m^2 \cdot g^{-1}$ respectively), supporting the successful polymer coating just at the external surface and not within the inner porosity.

In addition, the colloidal stability of the samples in aqueous solution before and after the surface functionalization was determined by dynamic light scattering (DLS, expressed as the average of the hydrodynamic value by number). The formation of large aggregates was reduced in CS@MIL-127 in comparison to noncoated MIL-127 (to 206 ± 87 nm from 455 ± 64 nm, respectively). This size variation could be

https://doi.org/10.1021/acsnano.1c10942
ACS Nano 2022, 16, 5830−5838

explained by the MOF surface charge modification, since neutral MIL-127 NPs (−1 ± 1 mV) tend to aggregate faster, while the cationic coating nature of CS@MIL-127 NPs (ζ-potential = +15 ± 1 mV) might afford an improved colloidal stability. Upon the CS coating, the surface charge modification (see Table 1) might be due to the presence of CS, bearing

Table 1. Particle Size (nm) and ζ-Potential (mV) for MIL-127 and CS@MIL-127 Obtained by DLS, in Water and Gastrointestinal (GI) Simulated Media[a]

	medium	MIL-127	CS@MIL-127
size (nm)	water	455 ± 64	206 ± 87
	lis-SIF	580 ± 26	201 ± 77
	lis-SIF-muc	589 ± 21	768 ± 30
	lis-SIF-panc	173 ± 84	223 ± 14
ζ-potential (mV)	water	−1 ± 0	+15 ± 1
	lis-SIF	−64 ± 1	0 ± 0
	lis-SIF-muc	−23 ± 1	−24 ± 0
	lis-SIF-panc	−7 ± 1	−10 ± 1

[a]Low-ionic-strength SIF (*lis*-SIF), *lis*-SIF-mucin (muc), and *lis*-SIF-pancreatin (panc).

protonated amino groups ($pK_a \approx 6.5$), supporting thus the location of CS moieties on the NPs' outer surface. Further pieces of evidence of the CS grafting were obtained by analyzing the MOF morphology by field-emission-gun scanning electron microscopy (FEG-SEM) images, corroborating the absence of morphological changes after CS coating (Figure S4).

NanoMOF Stability in Biorelevant Oral Conditions. Surface engineering is an emerging strategy for an efficient oral nanocarrier design, since it plays a crucial role on the biological affinity, governing not only mucoadhesiveness and tissue penetration but also activity and efficacy.[27] In this particular case, the expected grafting for a suitable oral formulation must be chemically robust and well-dispersed in the GI media for prolonged periods of time, enabling its action. In fact, we have already demonstrated a greater chemical stability under simulated oral conditions of a CS-coated MOF based on a different iron carboxylate MOF (MIL-100(Fe)).[26] In this line, the chemical, structural, and colloidal stability of MIL-127 and CS@MIL-127 were studied using different media, from the simplest media (water) to more complex simulated biorelevant GI media (at 37 °C; Figure 2): low-ionic-strength simulated intestinal media (*lis*-SIF), *lis*-SIF supplemented with pancreatin (*lis*-SIF-panc), a specific enzymatic mixture—amylases, lipases, and proteases—secreted by the pancreas into the intestine, or mucin (*lis*-SIF-muc), a glycosylated protein, which is the major macromolecular constituent of intestinal mucus.

Under simulated GI conditions, a stabilization of the CS-coated NPs is observed up to 24 h, with final particle sizes in *lis*-SIF-panc and *lis*-SIF-muc, respectively, of ∼170 and ∼590 nm (MIL-127) and ∼220 and ∼770 nm (CS@MIL-127). In both cases, the direct interaction of the media components (pancreatin or mucin) with the nanoMOF surface was evidenced by the shift to higher negative surfaces (−23 and −24 mV for MIL-127 and CS@MIL-127, respectively; Table 1) and the variation of the particle size (see a detailed discussion in the SI, Section S3), suggesting the formation of a protein corona,[28] which improves the colloidal stability of the nanoMOF.

Regarding the chemical stability, the release of the constitutive MOF linker was monitored by high-performance liquid chromatography (HPLC, Figure 2).

Indeed, the results demonstrated that the CS coating protects the MIL-127 framework from degradation, as the stability of the CS@MIL-127 is greater than the pristine MIL-127, particularly in *lis*-SIF and *lis*-SIF panc (e.g., *lis*-SIF panc 25 *vs.* 3% of linker release, respectively). Considering these results, we can conclude that CS coating effectively improves the chemical stability while maintaining the colloidal stability of MIL-127 NPs in simulated GI physiological media and could prevent the release of a future adsorbed drug.

Biosafety. One of the major challenges of novel nanoformulations and delivery strategies concerns their toxicity and immunogenicity.[29,30] In this sense, the influence of both CS-coated and uncoated NPs on the cellular toxicity was investigated against: (*i*) the murine macrophage cell line J774, as an appropriate model of the first defense line in the immune system against pathogens;[31] and (*ii*) Caco-2 human colorectal adenocarcinoma as an intestinal cell model, resembling the enterocytes lined in the small intestine, expressing their specific tight junctions, microvilli, and a large number of distinctive enzymes and transporters (peptidases, bile acids, etc.).[32] Further, the biocompatibility of MOFs was evaluated by using the *in vivo* model *C. elegans*. Aside from the similarities commented in the introduction, *C. elegans* allows a low-cost-effective initial biological assessment of nanoMOFs. The worm's transparency, small size, prolific and short lifecycle, few requirements for maintenance, and the possibility to use physicochemical techniques (e.g., HPLC) facilitate the in-deep study of the interactions between nanoMOFs and a multicellular organism.[33]

First, *in vitro* assays demonstrated that no significant differences were obtained by a cytotoxicity assay (MTT) over a wide range of concentrations (125 to 1000 $\mu g \cdot mL^{-1}$), from not only the MIL-127 and CS@MIL-127 NPs but also their individual precursors (CS, H_4TazBz, and $FeCl_3$). After 24 h of incubation, they exhibited a good biocompatibility with an inhibitory concentration (IC_{80} or the concentration inhibiting the growth of 20% of the cell population) of 800 $\mu g \cdot mL^{-1}$; Figure S6). These outcomes are in agreement with the absence of toxicity already demonstrated in other cell lines and other surface-engineered Fe-MOFs (e.g., MIL-100(Fe)).[26,34−36] Note also that the stability (colloidal, chemical, and structural) of the coated and noncoated NPs was evaluated in contact with supplemented cell culture media (DMEM), observing the preservation of their nanometric particle size and the negative surface charge due to the presence of proteins and/or antibiotics of the media (Figure S7).

Then, the potential toxicological character of MOFs was tested in *C. elegans*. MIL-127 and CS@MIL-127 were ingested by the worms: through the mouth, moving to the alimentary system, and posteriorly excreted. Drawing on the worms' transparency, we confirmed the ingestion of the MOFs by optical microscopy, directly visualizing the MOF aggregates along the intestinal tract (Figure 3A,D−G). Additionally, Prussian Blue staining (a blue dye specific for iron) confirmed the presence of iron within the intestinal tract (Figure S9). After inducing the excretion, no signs of Fe-MOFs were observed in the worms.

The biocompatibility of both nanoMOFs was studied by two toxicity parameters in young adult worms: survival and development (length analysis) after 24 h of exposure. We

https://doi.org/10.1021/acsnano.1c10942
ACS Nano 2022, 16, 5830−5838

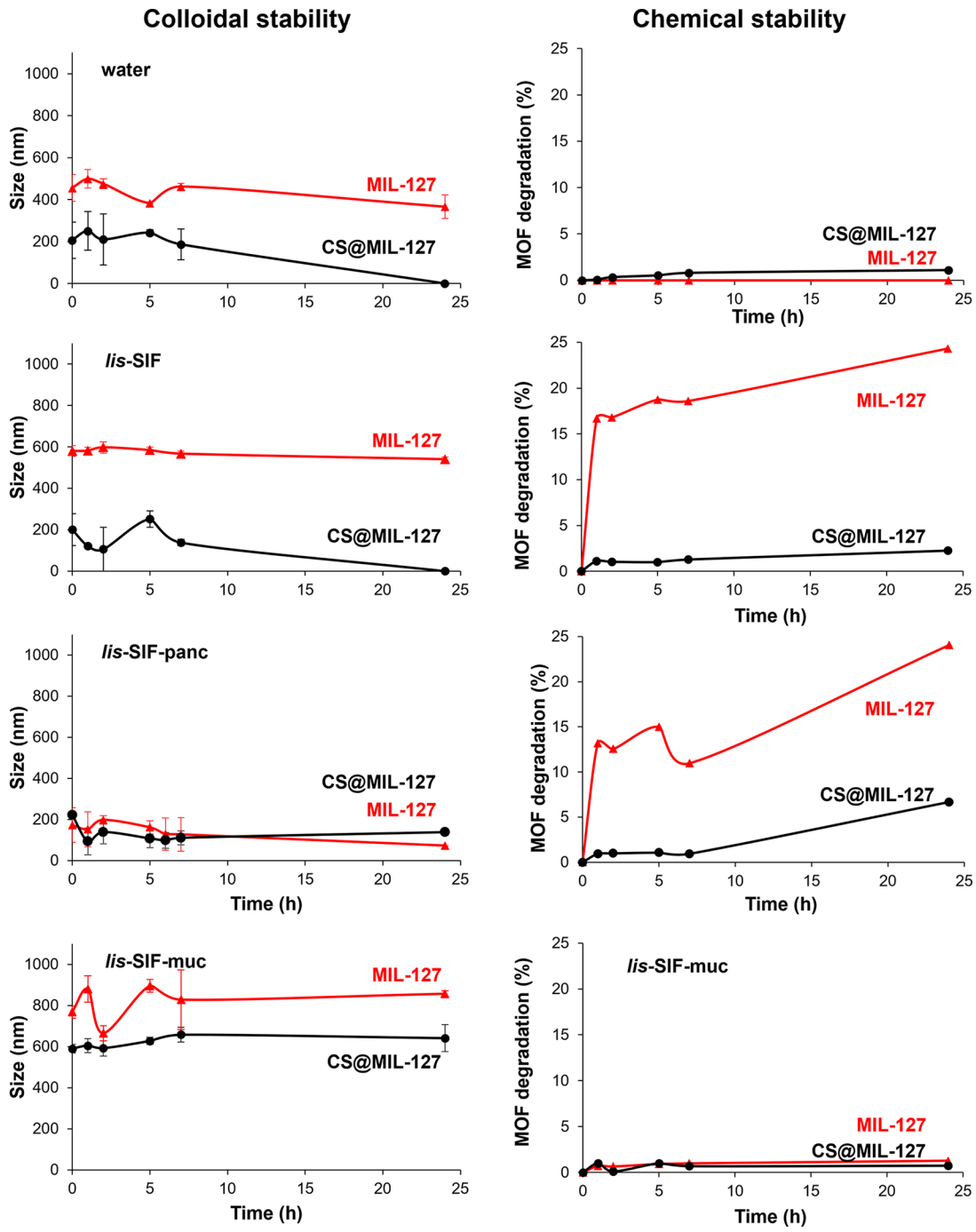

Figure 2. Colloidal stability and chemical stability of MIL-127 (red) and CS@MIL-127 (black) in water, *lis*-SIF, *lis*-SIF-panc, and *lis*-SIF-muc at 37 °C, representing the NP size evolution (nm; by DLS) or MOF degradation (%; by HPLC) *vs.* time (h).

assessed the MOFs' toxicity in the concentration range of 0–1000 $\mu g \cdot mL^{-1}$, observing that only the highest dose of CS@MIL-127 (1000 $\mu g \cdot mL^{-1}$) induced a slight decrease in the survival compared to the control group (Figure 3B), while the development was not affected in all studied concentrations. The survival and development were not affected when using MIL-127 NPs, supporting the biocompatibility on both nanosystems, in agreement with the previous cytotoxicity assays.

***In vivo C. elegans* Permeation.** In order to gain relevant and insightful information about the nanoMOF intestinal crossing, *in vivo* assays were performed using the model *C. elegans*; additionally, this amenable worm enabled us to perform extractions at different steps to evaluate by HPLC the content in the nanoMOFs. Worms were exposed to MIL-127 and CS@MIL-127 NPs in *lis*-SIF dispersions for 24 h (Figure 4). During feeding, *C. elegans* pumps liquids by rhythmic contractions of the pharynx to the lumen of the intestine.[37] Upon 24 h of exposure, the uptake of the nanoMOFs was quantified by HPLC (by means of the H_4TazBz linker, as previously for MOF degradation; see SI, Section S5), and it was found that *C. elegans* ingested statistically similar amounts of MIL-127 or CS@MIL-127 NPs (1.5 ± 0.1 and 1.0 ± 0.6%, respectively; see Figure 4). In

https://doi.org/10.1021/acsnano.1c10942
ACS Nano 2022, 16, 5830–5838

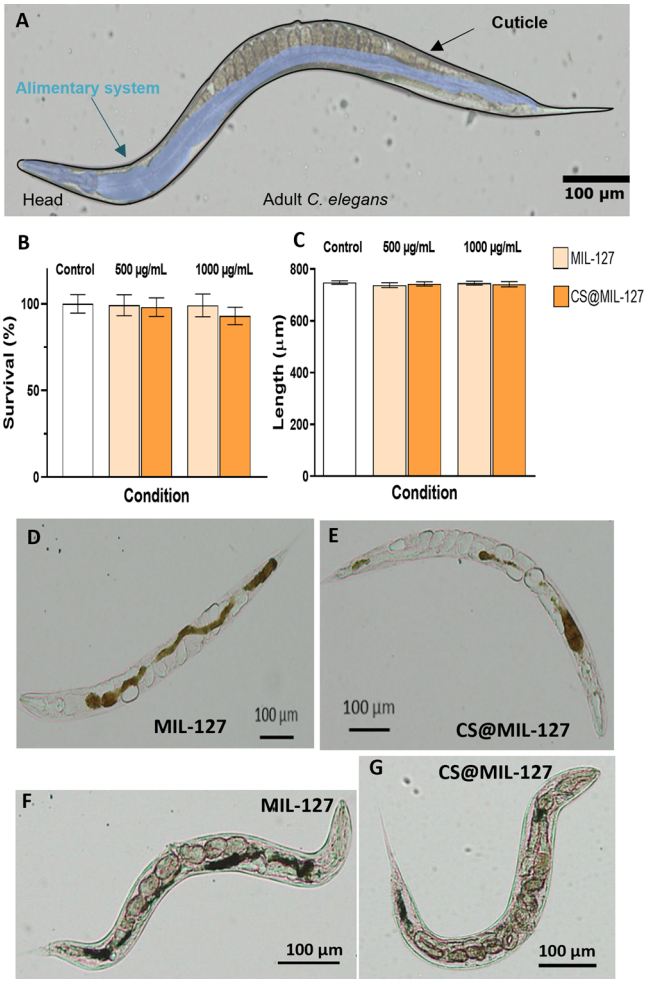

Figure 3. (A) Picture of an adult worm with the intestinal track highlighted in blue. (B) Graphical representation of the survival (%). (C) Length assay to assess the development in *C. elegans* after exposure to MIL-127 (flesh-colored) and CS@MIL-127 (orange) for 24 h at room temperature. Errors bars indicate the standard error of the mean (n = 3 independent experiments, used n = 300 worms). (D,E) Optical microscopy images of MIL-127- and CS@MIL-127-treated worms. (F,G) Optical microscopy images of adult worms after exposure to MIL-127 and CS@MIL-127 NPs stained with Prussian Blue. Areas with higher accumulation of NPs are seen; nanoMOFs are not seen in the cuticle.

terms of nanoMOF uptake per body mass, *C. elegans* ingested 35 ± 2 and 22 ± 4 g of MIL-127 and CS@MIL-127 per kg of worm, respectively, which is 35 and 22 orders of magnitude above the maximum dose administered to Wistar rats in previously reported detoxification studies using MIL-127 microparticles (1 $g{\cdot}kg^{-1}$).[38] These results emphasize that *C. elegans*, despite being a simple organism, can serve as a surrogate animal model for the *in vivo* MOF studies, being able to ingest doses exceeding other animal models.

After the nanoMOFs' oral administration to rats, it has been demonstrated that these materials can be excreted (e.g., MIL-127 or MIL-125-NH_2),[38,39] but no data about their intestinal absorption has been provided so far. As discussed in the Introduction, the nanoMOF oral absorption by the intestine could facilitate the drug administration in terms of stability and bioavailability, among others. To move beyond, we have here quantified the different absorption capacities of MIL-127 and CS@MIL-127 NPs in this *in vivo* model. After feeding worms

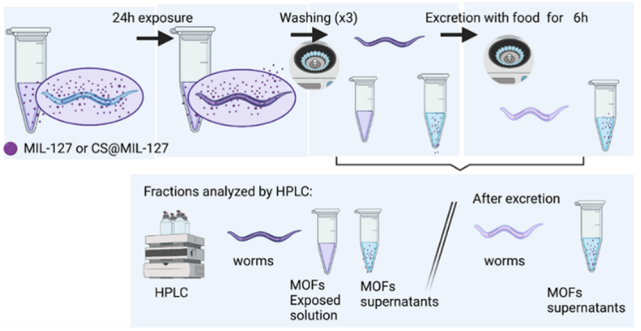

Table 1		Worms (%)	Remaining MOFs exposed solution (%)	MOFs Supernatant (%)
Ingested	MIL-127	1.5 ± 0.1	43.2 ± 13.9	89.4 ± 1.2
	CS@MIL-127	1.0 ± 0.6	65.8 ± 3.4	30.7 ± 16.4
Excreted	MIL-127	0.8 ± 0.3	-	0.4 ± 0.0
	CS@MIL-127	0.8 ± 0.3	-	0.9 ± 0.0

Figure 4. Scheme performed to study the ingestion and the excretion of nanoMOFs by *C. elegans* by HPLC. Table includes the HPLC results of MIL-127 and CS@MIL-127 uptake and excretion quantified. Note that the shown data correspond for each concentration to the average of triplicates obtained in three independent experiments (n = 3).

with the nanoMOFs, the amount of ingested material was quantified by first inducing the excretion of worms in a bacterial lawn (see SI, Section 5 for further details) and then quantifying the amount of absorbed nanoMOF in worms. The results show important differences in the worms' absorption of the MIL-127 and CS@MIL-127 NPs, being that the CS-coated NPs are more easily ingested by worms (53 vs. 80% of ingestion, respectively; Figure 4). These results support that the CS functionalization is an adequate strategy to increase the intestinal barrier bypass, enabling the absorption of nanoMOFs by the organism.

***Ex vivo* Permeation Studies.** For better understanding the nanoMOFs' intestinal bypass, a well-known *ex vivo* model based on Ussing permeation chambers (Ussing chamber) was used with a fresh functional rat intestine (Figure 5). Briefly, two compartments (donor and receptor), filled with simulated intestinal media, are separated by an intestinal biopsy (jejunum), allowing the easy monitoring of the nanoMOF crossing (see further details in the SI, Section 6). This

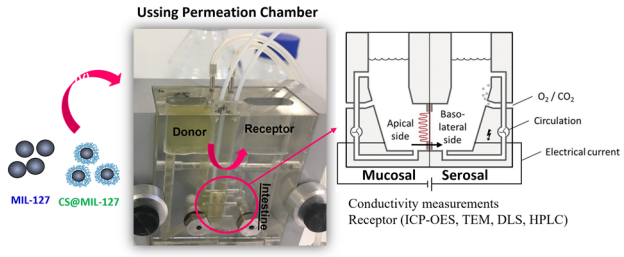

Figure 5. Shot and scheme of a Ussing permeation chamber used in the *ex vivo* experiments with the intestine of rat.[24] The tissue viability and integrity were controlled by monitoring the transepithelial resistance. From the receptor compartment, the collected aliquots were analyzed by HPLC (MOFs' constituents) as well as ICP-OES, TEM, and DLS (MOF NPs).

https://doi.org/10.1021/acsnano.1c10942
ACS Nano 2022, 16, 5830−5838

experimental design allows to track during the bypass process: (*i*) the particle size evolution of the nanosystems (DLS) in the donor and receptor compartments (Figure S8), (*ii*) the particle morphology by transmission electron microscopy (TEM) before and after crossing the intestine (Figure 6), (*iii*) the

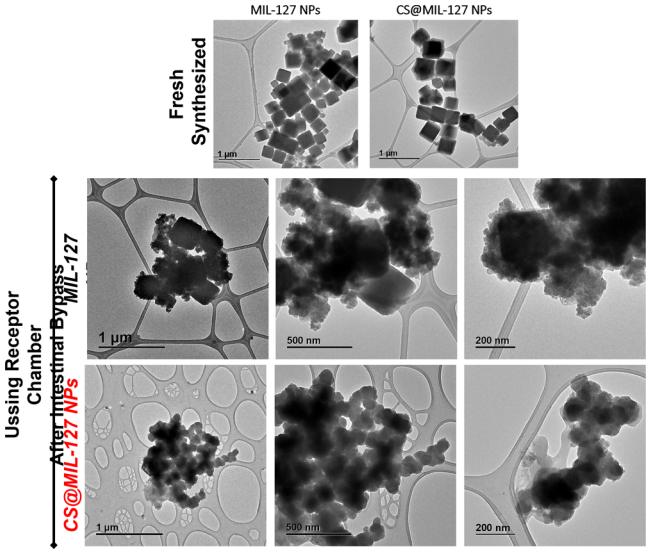

Figure 6. TEM images of MIL-127 and CS@MIL-127 NPs after their intestinal membrane bypass (samples recovered in the receptor Ussing chamber). TEM images of the fresh synthesized NPs of both solids are included for comparison. The scale bar corresponds to 200, 500, and 1000 nm.

histopathological examination of the intestine section (Prussian staining), visualizing both the tissue and the crossed NPs (Figure S9), and, finally, (*iv*) the viability of the intestinal membrane in contact with the NPs (see transepithelial resistance (TEER) measurements; Table S1).

To keep intact the integrity of the intestinal membrane, short contact times are usually applied (~2 h).[40] Thus, upon a 2 h exposure, a successful internalization across the intestinal tract was observed for both nanoMOFs regardless of the CS coating (9.5% absorbed NPs with a diffusion flux (F) and apparent permeability coefficient (P_{aap}) of 14.60 $\mu g \cdot cm^{-2} \cdot h^{-1}$ and 0.0073 $cm \cdot h^{-1}$, respectively). Compared with previous *in vivo* bypass (*C. elegans*), this lower intestinal intake could be due to the shorter contact.

Interestingly, the intestinal crossing was proven by the direct visualization of the NPs using TEM, observing the classical cubic morphology of MIL-127 NPs with a rounder shape than the pristine materials (Figure 6). The hydrodynamic size of the crossed nanoMOFs was comparable (~150 nm), in agreement with the observed similar intestinal bypass of both materials. However, the NPs' diameter in the donor chamber was initially larger for the CS-coated NPs than the uncoated ones (~392 vs. 214 nm, respectively; Figure S9), which might affect the intestinal bypass together with the surface nature. In addition, the different chemical stabilities of the nanoMOFs (7.5 and 0.9% degraded after 2 h in Ringer medium for MIL-127 and CS@MIL-127, respectively) could also influence the quantified NPs crossing coming from the nanoMOF constituents. However, in this particular case, this effect might be minimized by two facts: the low iron absorption in the distal jejunum (0.2 $\mu g \cdot cm^{-2} \cdot h^{-1}$)[41,42] and the experimentally determined null intake of the H_4TazBz ligand.

Moreover, the intestinal crossing was also confirmed with the histological sections: the nanoMOF presence was detected on the mucosa as well as within the tissue by using the Prussian blue staining (Figure S9). Further, this histological examination confirmed the absence of pathological changes with a normal tissue architecture, supporting the safety of both nanoMOFs. In this sense, the integrity of the intestinal membrane was also confirmed during the 2 h bypass by monitoring its polarization by TEER.[43] It should be noted that, compared to the control group, no significant differences were observed from all the tested formulations, in agreement with their good biocompatibility (Table S1).

CONCLUSIONS

The biocompatible and highly stable MIL-127 NPs can be absorbed through the intestinal barrier in relevant quantities, being further enhanced when coated with the biopolymer chitosan (53 vs. 80% of ingested MIL-127 and CS@MIL-127, respectively), as proven *in vivo* with the *C. elegans* model. This simple and relevant animal model was also used for demonstrating the biocompatibility of the uncoated and CS-coated nanoMOFs, even in the presence of very high doses, ingesting huge amounts of nanoMOFs (35 ± 2 and 22 ± 4 g of MIL-127 and CS@MIL-127 per kg of worm) when compared to other animal models. Further, *ex vivo* intestinal permeation studies supported a significant and rapid crossing of the intestinal barrier (9.5% in 2 h), ensuring not only their physicochemical properties (particle size, shape, and surface charge) but also their biocompatibility. These results provide relevant data for design of safe and efficient MOF oral drug delivery systems.

EXPERIMENTAL SECTION

Materials and Methods. All materials were commercially obtained and used without further purification. 5-Nitroisophtalic acid (98%), chitosan (CS) low molecular weight (~50 kDa, 75−80% acetylation degree (DA), 200−800 cP), pancreatin from porcine pancreas, albumin from bovine serum (lyophilized powder, ≥98%), heat-inactivated fetal bovine serum (FBS), mucin from porcine stomach (type III), phosphate buffered saline (PBS) solution (0.01 M, pH = 7.4), thiazolyl blue tetrazolium bromide (MTT: 3-(4,5-dimethylthiazol-2-yl)-2,5-diphenyltetrazolium bromide), α-D-glucose, and potassium ferricyanide(III) [$K_3Fe(CN)_6$] were purchased from Sigma-Aldrich. Dulbecco's Modified Eagle's Medium (DMEM) supplemented with glutamax-1, L-glutamine (2 mM), trypsin/ethylenediamine tetra-acetic acid (trypsin-EDTA, 10 mM, pH 7.4), penicillin/streptomycin (100 $U \cdot mL^{-1}$), and nonessential amino acids (100×) dimethyl sulfoxide (DMSO; ≥99.7%) were purchased from Fisher.

Synthesis of MIL-127 and CS@MIL-127 Nanoparticles (NPs). MIL-127 NPs were synthesized following previously reported procedures.[25] The ligand 3,3′,5,5′-azobenzenetetracarboxylic acid (H_4TazBz) was first synthesized. 5-Nitroisophthalic acid (19 g, 90 mmol) and NaOH (50 g, 1250 mmol) were mixed in 250 mL of distilled water and placed into a 1 L three-neck round-bottom flask under vigorous stirring at 60 °C. D-Glucose (100 g) was dissolved in 150 mL of water and added to this slurry solution. After the mixture cooled down to room temperature (RT), airflow was bubbled into the brown mixture for 4 h under stirring. After the mixtured cooled down in an ice-bath, the disodium salt was recovered by filtration and washed with a small amount of cold water. The resulting yellow solid was then dissolved in 200 mL of distilled water, and this solution was acidified to pH = 1 by the addition of HCl (37%). The resulting orange solid was recovered by filtration, washed with water, and dried at 100 °C under vacuum.

https://doi.org/10.1021/acsnano.1c10942
ACS Nano 2022, 16, 5830−5838

Synthesis of CS@MIL-127. The coating of the outer surface of MIL-127 NPs was performed using a simple and completely green one-pot impregnation method, adapted from one recently developed by some of us.[26] MIL-127 NPs (30 mg; note here that NPs were used wet, so the wet amount of material was previously determined from NPs dried at 100 °C overnight) were dispersed in 6 mL of ethanol using an ultrasound tip. In a different vial, 32 mg of chitosan (CS) was suspended in 7 mL of distilled water. Then, suspensions were mixed and kept under stirring for 30 min. The molar ratio between MIL-127 NPs and CS in the reaction mixture was 58:1, with MIL-127 and CS concentrations of 2.3 and 2.5 mg·mL^{-1}, respectively. The CS-coated NPs were collected by centrifugation and washed with aliquots of 15 mL of AcOH 1% (v/v) (1×) and water (5×). Finally, the product was stored wet in water.

Preparation of Physiological Simulated Media. *Phosphate Buffer Saline (PBS, pH = 7.4).* A 0.01 M phosphate buffer saline (0.138 M NaCl and 0.003 M KCl), pH = 7.4, solution was used.

Lis-SIF (Low-Ionic-Strength SIF). NaOH solution (1.54 mL, 0.02 M) was added to a solution of 136 mg of KH_2PO_4 dissolved in 125 mL of Milli-Q water. Then, Milli-Q water was added until a volume of 500 mL to finally adjust the pH to 6.8 with 2 M NaOH (see Table 2). Prior to the analysis, the biological media were kept at 37 °C.

Table 2. Composition of Intestinal Simulated Media

	supplemented *lis*-SIF	
composition	conc (mM)	g per 500 mL
NaOH	0.6	0.012
KH_2PO_4	2.0	0.136
pancreatin	—	5
mucin	—	25
pH	6.8	

Lis-SIF-panc. *Lis*-SIF supplemented with pancreatin was prepared by dissolving the pancreatin at 1% w/v in *lis*-SIF and stirring the mixture for 3 h. Then, the solution was centrifuged (14 000 rpm, 10 min) to eliminate pancreatin aggregates. Note that the final pancreatin concentration of 1% is rather an estimated value.

Lis-SIF-muc. *Lis*-SIF supplemented with mucin was prepared by dissolving the mucin at 5% w/v in *lis*-SIF,[44] keeping the mixture under magnetic stirring for 3.5 h. Then, 330 μL of this solution was diluted in 10 mL of *lis*-SIF.

Ringer Solution. Ringer solution was prepared by mixing 50 mL of aqueous solution 1 (see Table 3), 100 mL of aqueous solution 2,

Table 3. Composition of Solution 1 and Solution 2 Used for the Preparation of Ringer Medium[a]

solution 1		
salt	weight (g)	concentration (mM)
$MgCl_2·6H_2O$	4.82	1.2
$CaCl_2·2H_2O$	3.52	1.2
solution 2		
salt	weight (g)	concentration (mM)
K_2HPO_4	4.16	2.4
KH_2PO_4	0.54	0.4

[a]Volumes were adjusted to 1000 mL with Milli-Q water.

NaCl (6.72 g), and $NaHCO_3$ (2.10 g). The final volume of the Ringer medium was adjusted to 1000 mL with Milli-Q water. The compositions of solutions 1 and 2 are indicated in Table 3. The pH was adjusted to 6.00 with a 2 M HCl solution.[45]

ASSOCIATED CONTENT

Supporting Information

The Supporting Information is available free of charge at https://pubs.acs.org/doi/10.1021/acsnano.1c10942.

Experimental techniques, MIL-127 and CS@MIL-127 characterization, MOF stability under diverse physiological media, *in vitro* cell studies, *in vivo* studies: *C. elegans*, *ex vivo* studies: intestinal permeability, and statistics (PDF)

AUTHOR INFORMATION

Corresponding Authors

Patricia Horcajada − *Advanced Porous Materials Unit (APMU), IMDEA Energy Institute, 28935 Móstoles-Madrid, Spain;* orcid.org/0000-0002-6544-5911; Email: patricia.horcajada@imdea.org

Anna Laromaine − *Institut de Ciència de Materials de Barcelona (ICMAB-CSIC), 08193 Bellaterra, Spain;* orcid.org/0000-0002-4764-0780; Email: alaromaine@icmab.es

Authors

Sara Rojas − *Advanced Porous Materials Unit (APMU), IMDEA Energy Institute, 28935 Móstoles-Madrid, Spain;* Present Address: Department of Inorganic Chemistry, University of Granada, Av. Fuentenueva S/N, 18071 Granada, Spain. (S.R.); orcid.org/0000-0002-7874-2122

Tania Hidalgo − *Advanced Porous Materials Unit (APMU), IMDEA Energy Institute, 28935 Móstoles-Madrid, Spain;* orcid.org/0000-0002-3498-9967

Zhongrui Luo − *Institut de Ciència de Materials de Barcelona (ICMAB-CSIC), 08193 Bellaterra, Spain*

David Ávila − *Department of Inorganic Chemistry, Chemical Sciences Faculty, Complutense University of Madrid, 28040 Madrid, Spain*

Complete contact information is available at: https://pubs.acs.org/10.1021/acsnano.1c10942

Funding

CS functionalization was cofunded by Ramón Areces Foundation project H+MOFs and the M-ERA-NET C-MOF.cell project (PCI2020−111998 funded by MCIN/AEI/10.13039/501100011033 and by the European Union NextGenerationEU/PRTR). The authors acknowledge "Comunidad de Madrid" and European Regional Development Fund-FEDER 2014-2020-OE REACT-UE 1 for their financial support to the VIRMOF-CM project associated with R&D projects in response to COVID-19. This research publication is also part of the projects RTI2018-096273-B-I00 founded by MCIN/AEI/ /10.13039/501100011033/FEDER "Una manera de hacer Europa", PID2019−104228RB-I00 founded by MCIN/AEI/10.13039/501100011033, PID2020−112848RB-C21 founded by MCIN/AEI/10.13039/501100011033, the Generalitat de Catalunya (2017SGR765), the "Severo Ochoa" Programme for Centres of Excellence in R&D (SEV-2015-0496 and CEX2019-000917-S), Regional Madrid funding (Talento 2017 Modality 2, 2017-T2/IND-5149), Juan de la Cierva incorporation grant JC2019-038894-I founded by MCIN/AEI/10.13039/501100011033, and by the European Union NextGenerationEU/PRTR, Multifunctional Metallodrugs in Diagnosis and Therapy Network (MICIU, RED2018-102471-T). A.L. participates in the networks of EPNOE, Red Nanocare RED2018-102469-T, and the CSIC Interdisciplinary Platform for Sustainable Plastics toward a Circular Economy, SUSPLAST.

Notes

The authors declare no competing financial interest.

REFERENCES

(1) Horcajada, P.; Serre, C.; Vallet-Regí, M.; Sebban, M.; Taulelle, F.; Férey, G. Metal-Organic Frameworks as Efficient Materials for Drug Delivery. *Angew. Chem., Int. Ed.* **2006**, *45*, 5974−5978.

(2) Li, H.; Eddaoudi, M.; O'Keeffe, M.; Yaghi, O. M. Design and Synthesis of an Exceptionally Stable and Highly Porous Metal-Organic Frameworks. *Nature* **1999**, *402* (18), 276−279.

(3) Velásquez-Hernández, M. de J.; Linares-Moreau, M.; Astria, E.; Carraro, F.; Alyami, M. Z.; Khashab, N. M.; Sumby, C. J.; Doonan, C. J.; Falcaro, P. Towards Applications of Bioentities@MOFs in Biomedicine. *Coord. Chem. Rev.* **2021**, *429*, 213651.

(4) Fernández-Paz, C.; Rojas, S.; Salcedo-Abraira, P.; Simón-Yarza, T.; Remuñán-López, C.; Horcajada, P. Metal-Organic Framework Microsphere Formulation for Pulmonary Administration. *ACS Appl. Mater. Interfaces* **2020**, *12* (23), 25676−25682.

(5) Santos, J. H.; Quimque, M. T. J.; Macabeo, A. P. G.; Corpuz, M. J. T.; Wang, Y.; Lu, T.; Lin, C.; Villaflores, O. B. Enhanced Oral Bioavailability of the Pharmacologically Active Lignin Magnolol via Zr-Based Metal Organic Framework Impregnation. *Pharmaceutics* **2020**, *12*, 437.

(6) Márquez, A. G.; Hidalgo, T.; Lana, H.; Cunha, D.; Blanco-Prieto, M. J.; Álvarez-Lorenzo, C.; Boissière, C.; Sánchez, C.; Serre, C.; Horcajada, P. Biocompatible Polymer-Metal-Organic Framework Composite Patches for Cutaneous Administration of Cosmetic Molecules. *J. Mater. Chem. B* **2016**, *4*, 7031−7040.

(7) Gandara-Loe, J.; Ortuno-Lizarán, I.; Fernández-Sanchez, L.; Alió, J. L.; Cuenca, N.; Vega-Estrada, A.; Silvestre-Albero, J. Metal-Organic Frameworks as Drug Delivery Platforms for Ocular Therapeutics. *ACS Appl. Mater. Interfaces* **2019**, *11* (2), 1924−1931.

(8) Taherzade, S. D.; Rojas, S.; Soleimannejad, J.; Horcajada, P. Combined Cutaneous Therapy Using Biocompatible Metal-Organic Frameworks. *Nanomaterials* **2020**, *10*, 2296−2316.

(9) Hartlieb, K. J.; Ferris, D. P.; Holcroft, J. M.; Kandela, I.; Stern, C. L.; Nassar, M. S.; Botros, Y. Y.; Stoddart, J. F. Encapsulation of Ibuprofen in CD-MOF and Related Bioavailability Studies. *Mol. Pharmaceutics* **2017**, *14*, 1831−1839.

(10) Miao, Y. B.; Pan, W. Y.; Chen, K. H.; Wei, H. J.; Mi, F. L.; Lu, M. Y.; Chang, Y.; Sung, H. W. Engineering a Nanoscale Al-MOF-Armored Antigen Carried by a "Trojan Horse"-Like Platform for Oral Vaccination to Induce Potent and Long-Lasting Immunity. *Adv. Funct. Mater.* **2019**, *29* (43), 1904828.

(11) Zhou, Y.; Liu, L.; Cao, Y.; Yu, S.; He, C.; Chen, X. A Nanocomposite Vehicle Based on Metal - Organic Framework Nanoparticle Incorporated Biodegradable Microspheres for Enhanced Oral Insulin Delivery. *ACS Appl. Mater. Interfaces* **2020**, *12* (20), 22581−22592.

(12) Botet-Carreras, A.; Tamames-Tabar, C.; Salles, F.; Rojas, S.; Imbuluzqueta, E.; Lana, H.; Blanco-Prieto, M. J.; Horcajada, P. Improving the Genistein Oral Bioavailability via Its Formulation into the Metal-Organic Framework MIL-100(Fe). *J. Mater. Chem. B* **2021**, *9*, 2233−2239.

(13) Hua, S. Advances in Oral Drug Delivery for Regional Targeting in the Gastrointestinal Tract - Influence of Physiological, Pathophysiological and Pharmaceutical Factors. *Front. Pharmacol.* **2020**, *11* (April), 1−22.

(14) McGhee, J. D. The C. elegans intestine. *WormBook*, 2007. http://www.wormbook.org/chapters/www_intestine/intestine.html.

(15) Gonzalez-Moragas, L.; Berto, P.; Vilches, C.; Quidant, R.; Kolovou, A.; Santarella-Mellwig, R.; Schwab, Y.; Stürzenbaum, S.; Roig, A.; Laromaine, A. In Vivo Testing of Gold Nanoparticles Using the Caenorhabditis Elegans Model Organism. *Acta Biomater.* **2017**, *53*, 598−609.

(16) Dhakshinamoorthy, A.; Alvaro, M.; Chevreau, H.; Horcajada, P.; Devic, T.; Serre, C.; Garcia, H. Iron(III) Metal-Organic Frameworks as Solid Lewis Acids for the Isomerization of α-Pinene Oxide. *Catal. Sci. Technol.* **2012**, *2*, 324−330.

(17) Tamames-Tabar, C.; Cunha, D.; Imbuluzqueta, E.; Ragon, F.; Serre, C.; Blanco-Prieto, M. J.; Horcajada, P. Cytotoxicity of Nanoscaled Metal-Organic Frameworks. *J. Mater. Chem. B* **2014**, *2*, 262−271.

(18) Rojas, S.; Colinet, I.; Cunha, D.; Hidalgo, T.; Salles, F.; Serre, C.; Guillou, N.; Horcajada, P. Toward Understanding Drug Incorporation and Delivery from Biocompatible Metal-Organic Frameworks in View of Cutaneous Administration. *ACS Omega* **2018**, *3*, 2994−3003.

(19) Cunha, D.; Ben Yahia, M.; Hall, S.; Miller, S. R.; Chevreau, H.; Elkaim, E.; Maurin, G.; Horcajada, P.; Serre, C. Rationale of Drug Encapsulation and Release from Biocompatible Porous Metal - Organic Frameworks. *Chem. Mater.* **2013**, *25*, 2767−2776.

(20) Chevreau, H.; Permyakova, A.; Nouar, F.; Fabry, P.; Livage, C.; Ragon, F.; Garcia-Marquez, A.; Devic, T.; Steunou, N.; Serre, C.; Horcajada, P. Synthesis of the Biocompatible and Highly Stable MIL-127(Fe): From Large Scale Synthesis to Particle Size Control. *CrystEngComm* **2016**, *18*, 4094−4101.

(21) Patel, J.; Patel, A. Toxicity of Nanomaterials on the Liver, Kidney, and Spleen. *Biointeractions of Nanomaterials*, 1st ed.; CRC Press, 2015; pp 286−306.

(22) Lang, X.; Wang, T.; Sun, M.; Chen, X.; Liu, Y. Advances and Applications of Chitosan-Based Nanomaterials as Oral Delivery Carriers: A Review. *Int. J. Biol. Macromol.* **2020**, *154*, 433−445.

(23) Rostami, E. Progresses in Targeted Drug Delivery Systems Using Chitosan Nanoparticles in Cancer Therapy: A Mini-Review. *J. Drug Delivery Sci. Technol.* **2020**, *58*, 101813.

(24) Westerhout, J; Wortelboer, H; Verhoeckx, K. Ussing Chamber. *The Impact of Food Bioactives on Health* **2015**, 263.

(25) Chevreau, H.; Permyakova, A.; Nouar, F.; Fabry, P.; Livage, C.; Ragon, F.; Garcia-Marquez, A.; Devic, T.; Steunou, N.; Serre, C.; Horcajada, P. Synthesis of the Biocompatible and Highly Stable MIL-127(Fe): From Large Scale Synthesis to Particle Size Control. *CrystEngComm* **2016**, *18* (22), 4094−4101.

(26) Hidalgo, T.; Giménez-Marqués, M.; Bellido, E.; Avila, J.; Asensio, M. C.; Salles, F.; Lozano, M. V.; Guillevic, M.; Simón-Vázquez, R.; González-Fernández, A.; Serre, C.; Alonso, M. J.; Horcajada, P. Chitosan-Coated Mesoporous MIL-100(Fe) Nanoparticles as Improved Bio-Compatible Oral Nanocarriers. *Sci. Rep.* **2017**, *7*, 43099−43113.

(27) Frank, L. A.; Onzi, G. R.; Morawski, A. S.; Pohlmann, A. R.; Guterres, S. S.; Contri, R. V. Chitosan as a Coating Material for Nanoparticles Intended for Biomedical Applications. *React. Funct. Polym.* **2020**, *147*, 104459.

(28) Meyers, S. R.; Grinstaff, M. W. Biocompatible and Bioactive Surface Modifications for Prolonged in Vivo Efficacy. *Chem. Rev.* **2012**, *112* (3), 1615−1632.

(29) Perciani, C. T.; Liu, L. Y.; Wood, L.; Macparland, S. A. Enhancing Immunity with Nanomedicine: Employing Nanoparticles to Harness the Immune System. *ACS Nano* **2021**, *15* (1), 7−20.

(30) Naran, K.; Nundalall, T.; Chetty, S.; Barth, S. Principles of Immunotherapy: Implications for Treatment Strategies in Cancer and Infectious Diseases. *Front. Microbiol.* **2018**, *9*, 3158.

(31) Hirayama, D.; Iida, T.; Nakase, H. The Phagocytic Function of Macrophage-Enforcing Innate Immunity and Tissue Homeostasis. *Int. J. Mol. Sci.* **2018**, *19*, 92.

(32) Hidalgo, I. J.; Raub, T. J.; Borchardt, R. T. Characterization of the Human Colon Carcinoma Cell Line (Caco-2) as a Model System for Intestinal Epithelial Permeability. *Gastroenterology* **1989**, *96* (2), 736−749.

(33) Gonzalez-Moragas, L.; Roig, A.; Laromaine, A. C. Elegans as a Tool for in Vivo Nanoparticle Assessment. *Adv. Colloid Interface Sci.* **2015**, *219*, 10−26.

(34) Giménez-Marqués, M.; Bellido, E.; Berthelot, T.; Simón-Yarza, T.; Hidalgo, T.; Simón-Vázquez, R.; González-Fernández, Á.; Avila, J.; Asensio, M. C.; Gref, R.; Couvreur, P.; Serre, C.; Horcajada, P. GraftFast Surface Engineering to Improve MOF Nanoparticles Furtiveness. *Small* **2018**, *14* (40), 1801900.

https://doi.org/10.1021/acsnano.1c10942
ACS Nano 2022, 16, 5830−5838

(35) Agostoni, V.; Horcajada, P.; Noiray, M.; Malanga, M.; Aykaç, A.; Jicsinszky, L.; Vargas-Berenguel, A.; Semiramoth, N.; Daoud-Mahammed, S.; Nicolas, V.; Martineau, C.; Taulelle, F.; Vigneron, J.; Etcheberry, A.; Serre, C.; Gref, R. A "'Green"' Strategy to Construct Non-Covalent, Stable and Bioactive Coatings on Porous MOF Nanoparticles. *Sci. Rep.* **2015**, *5*, 1−7.
(36) Bellido, E.; Hidalgo, T.; Lozano, M. V.; Guillevic, M.; Simón-Vázquez, R.; Santander-Ortega, M. J.; González-Fernández, A.; Serre, C.; Alonso, M. J.; Horcajada, P. Heparin-Engineered Mesoporous Iron Metal-Organic Framework Nanoparticles: Toward Stealth Drug Nanocarriers. *Adv. Healthc. Mater.* **2015**, *4*, 1246−1257.
(37) Hall, D. H.; Altun, Z. F. *C. elegans Atlas*, 1st ed.; Cold Spring Harbor Laboratory Press: New York, 2008.
(38) Rojas, S.; Baati, T.; Njim, L.; Manchego, L.; Neffati, F.; Abdeljelil, N.; Saguem, S.; Serre, C.; Najjar, M. F.; Zakhama, A.; Horcajada, P. Metal-Organic Frameworks as Efficient Oral Detoxifying Agents. *J. Am. Chem. Soc.* **2018**, *140* (30), 9581−9586.
(39) Rojas, S.; Guillou, N.; Horcajada, P. Ti-Based NanoMOF as an Efficient Oral Therapeutic Agent. *ACS Appl. Mater. Interfaces* **2019**, *11*, 22188−22193.
(40) Clarke, L. L. A Guide to Ussing Chamber Studies of Mouse Intestine. *Am. J. Physion Gastroinstest Liver Physiol* **2009**, *296*, G1151−G1166.
(41) Tandy, S.; Williams, M.; Leggett, A.; Lopez-Jimenez, M.; Dedes, M.; Ramesh, B.; Srai, S. K.; Sharp, P. Nramp2 Expression Is Associated with PH-Dependent Iron Uptake across the Apical Membrane of Human Intestinal Caco-2 Cells. *J. Biol. Chem.* **2000**, *275* (2), 1023−1029.
(42) Gulec, S.; Anderson, G. J.; Collins, J. F. Mechanistic and Regulatory Aspects of Intestinal Iron Absorption. *Am. J. Physiol. - Gastrointest. Liver Physiol.* **2014**, *307* (4), G397.
(43) Haslam, I. S.; O'Reilly, D. A.; Sherlock, D. J.; Kauser, A.; Womack, C.; Coleman, T. Pancreatoduodenectomy as a Source of Human Small Intestinefor Ussing Chamber Investigations and Comparative Studieswith Rat Tissue. *Biopharm. Drug Dispos.* **2011**, *32*, 210−221.
(44) Lai, S. K.; Wang, Y.; Wirtz, D.; Hanes, J. Micro- and Macrorheology of Mucus. *Adv. Drug Delivery Rev.* **2009**, *61*, 86−100.
(45) Mazzaferro, S.; Bouchemal, K.; Skanji, R.; Gueutin, C.; Chacun, H.; Ponchel, G. Intestinal Permeation Enhancement of Docetaxel Encapsulated into Methyl-β-Cyclodextrin/Poly-(Isobutylcyanoacrylate) Nanoparticles Coated with Thiolated Chitosan. *J. Controlled Release* **2012**, *162*, 568−574.

https://doi.org/10.1021/acsnano.1c10942
ACS Nano 2022, 16, 5830−5838